

Open-loop shaping of a 4K MEMS with Fourier-domain pre-compensation

Lisa A. Poyneer

Lawrence Livermore National Laboratory, 7000 East Avenue, Livermore, California 94550

poyneer1@llnl.gov

Andrew Norton and Daren Dillon

*UCO Lick Observatory, Laboratory for Adaptive Optics,
University of California, Santa Cruz,*

1156 High Street, Santa Cruz, California 95064, USA

apnorton@ucsc.edu, dillon@ucolick.org

Abstract: We describe a computationally efficient Fourier-domain algorithm for influence function compensation and an improved voltage-phase calibration technique that together enable precise open-loop shaping of a 64×64 MEMS deformable mirror.

© 2009 Optical Society of America

OCIS codes: (010.1080) Adaptive Optics, (230.6120) Spatial Light Modulators

1. Introduction

For both closed-loop and open-loop high performance Adaptive Optics (AO) applications, it is essential that the desired phase correction can be shaped on the deformable mirror (DM) in a single step. In our recent work for the Gemini Planet Imager (GPI) we have focused on developing a computationally efficient algorithm for MEMS shaping. Since GPI will use Fourier Transform wavefront reconstruction (FTR) [1], a Fourier-domain approach was chosen. The response of the MEMS actuators is pre-compensated for by the use of a Fourier-domain filter that is based on the influence function. In our initial tests [2] with a 32×32 Boston micromachines (BMC) MEMS, we demonstrated that this filtering approach, when combined with voltage-phase quadratic calibration of the actuators [3], removed most, but not all, of the open-loop shaping error.

Since these test we have further refined our work. With a new, higher-stroke 64×64 BMC MEMS available, we can now form a full typical GPI Tweeter phase, which we could not do with the 32×32 MEMS in either number of actuators or stroke. Second, we have modified our voltage-phase calibration technique. Third, we have refined our pre-compensation filter calculation. With these improved techniques and new MEMS, we can form a variety of GPI Tweeter shapes (ranging from 258 to 301 nm RMS) with only 25 to 31 nm RMS error in the controllable spatial frequencies. We address these three issues and then give experimental results.

2. New MEMS and new algorithms

We eschew developing a plate-equation or fundamental physics model of the MEMS device and instead use a simple metric to characterize the nonlinearity of the MEMS device. We term this metric “two-poke nonlinearity”. If linear superposition held, the phase made by poking two neighboring actuators would be exactly the sum of the phases made by poking each actuator individually. The two-poke nonlinearity is the amount that the peak height of the actual phase differs from the linear superposition model. This is determined for an actual device by holding the mirror at bias voltage (110 V for our device), and then moving the actuators either above bias (up to 160 V) to generate positive displacements or below bias (down to 0 V) to generate negative displacements.

We had used this measurement to characterize the 32×32 MEMS in our initial work [2] and found that that device had $\pm 2\%$ nonlinearity at maximum displacement away from flat. For high voltages, linear superposition slightly over-estimates the peak phase; for low voltages linear superposition slightly under-estimates the peak phase. We repeated this test with the 64×64 MEMS. For the same peak displacement (which is achieved at a lower voltage differential from bias) the new mirror had the same $\pm 2\%$ nonlinearity as the old one. For larger displacements, the new 64×64 MEMS exhibited two important differences. First, the two-poke nonlinearity is up to 5% for maximum voltages.

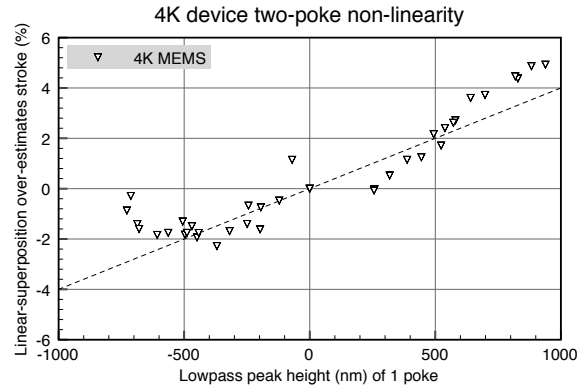


Fig. 1. [Left] Two-poke nonlinearity of the 64×64 MEMS. Positive peak heights (x-axis) are for voltages greater than bias (110 to 160 V); negative are for voltages less than bias (0 to 110 V). For high voltage the nonlinearity is $\sim 5\%$ at 1 micron stroke; at very high and very low voltage the behavior is strongly asymmetric.

Second, the behavior is not symmetric - for the lowest voltages the two-poke nonlinearity is relatively uniform around 2%. The data are shown in Figure 1.

As described in [2], Section 3, the influence function of the MEMS fully characterizes its frequency response, assuming that the device is linear, shift-invariant. In our initial test we took a high-resolution interferometric measurement of the influence function and fit it with the model of Vogel and Yang[4]. This signal was then sampled correctly and numerically transformed with the Discrete Fourier Transform (DFT) to obtain the pre-compensation filter.

For the 64×64 device we instead took a high-resolution interferometric measurement of the influence function, resampled it appropriately, then calculated the DFT. In the frequency domain we fit a two-part Gaussian model. For the model a Gaussian is specified in the actuator domain. Indexing the 64×64 signal with frequencies k and l from -32 to 31 , we fit the inner region $\sqrt{k^2 + l^2} \leq 16$ with a Gaussian with standard deviation 0.7 actuator spacings. For the remaining high spatial frequencies, a Gaussian with standard deviation 0.5 actuator spacings gave the best fit.

Previously we had used a threshold to limit the amplification of high spatial frequencies to a factor of 10. Here we found that not using this limit resulted in best open-loop shaping performance.

The quadratic relationship between applied actuator voltage and measured peak actuator phase displacement has been calibrated for our MEMS devices by using the raw (all spatial frequencies) peak phase as measured by our interferometer [3]. However, since we desired to form a phase shape only within the controllable spatial frequency range of the MEMS, this calibration should be done instead with the lowpass-filtered phase. A comparison of using the raw peak height and the lowpass height is shown in Fig. 2. For low voltages, the calibrations differ by nearly 200 nm. Using this new voltage-phase calibration significantly improved our open-loop shaping performance.

3. Experimental results

Eight different GPI Tweeter shapes were generated using the GPI simulation code for a median r_0 atmosphere controlled in closed loop. Each signal $\phi[x, y]$ was shaped on the mirror as both $\phi[x, y]$ and $-\phi[x, y]$ to help assess the impact of the asymmetry in two-poke nonlinearity. The algorithm to generate actuator voltages from the desired phase $\phi[x, y]$ is simple. The phase $\phi[x, y]$ is DFTed, divided by the influence function filter, and then inverse DFTed. For each actuator phase, the new quadratic voltage-phase calibration is reversed to obtain voltages.

Results are given in Table 1. The in-band RMS shaping error for ϕ and $-\phi$ are given and then the RMS difference between the two. The efficacy of the new lowpass voltage-phase calibration is clear in the reduced RMS shaping error. The asymmetry of the two-poke nonlinearity plays a role in the fact that the difference between shaping ϕ and $-\phi$ is between 31 and 40 nm. Exactly how much has not yet been determined.

4. Conclusions and future work

We have demonstrated 30 nm RMS open-loop shaping of 300 nm RMS mid-frequency atmospheric turbulence for the GPI scenario. This is achieved in a computationally efficient manner with a Fourier-domain pre-compensation filter and improved voltage-phase calibration. The 64×64 device exhibits -2% to 5% two-poke nonlinearity, contributing

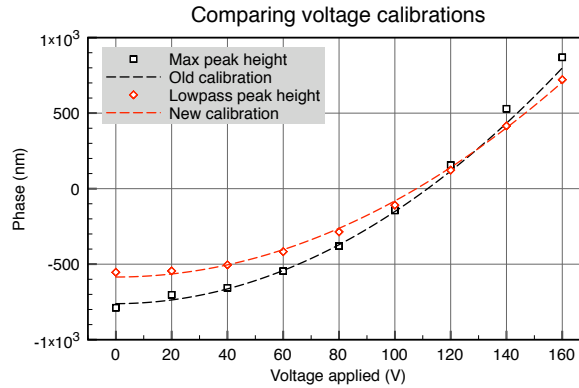


Fig. 2. The old voltage-phase calibration (black dashed curve) was done based on the maximum heights of poked actuators (black squares). The actual lowpass peak height is about 20% lower. For the new calibration, the displacements of the lowpass-filtered peaks (red diamonds) are fit instead (red dashed line). The two calibrations differ by 176 nm at 0 V.

Table 1. Open-loop shaping performance and \pm shaping differences (all in in-band RMS (nm)). Eight different GPI closed-loop Tweeter phases were used. With old calibration and DM compensation filter, the open-loop error median was 37 nm and the plus-minus error median was 56 nm. With the new voltage calibration, the shaping error is reduced to a median of 30 nm (23 nm reduction) and the plus-minus error median to 34 nm (45 nm reduction). All error terms are in-band RMS.

Input (nm)		MEMS errors (nm)					
Peak-Valley	RMS	Old calibration			New calibration		
		$+\phi$	$-\phi$	$\pm\phi$ diff	$+\phi$	$-\phi$	$\pm\phi$ diff
1844	291	49	39	77	25	25	34
2026	296	34	35	50	29	32	38
2113	301	36	37	46	32	35	39
1705	258	24	29	31	24	30	31
2052	271	32	30	32	31	31	34
1918	303	35	38	56	29	31	40
1951	283	38	53	78	28	30	34
1897	268	42	54	79	27	31	33

to the fact that shaping a phase $\phi[x,y]$ and its negative $-\phi[x,y]$ is done with up to 40 nm RMS error between the shapes. In future work we will explore further refinements to the model fit of the influence function pre-compensation filter and test closed-loop convergence performance.

Acknowledgments

This work was performed under the auspices of the U.S. Department of Energy by the University of California, Lawrence Livermore National Laboratory under contract No. W-7405-Eng-48. The document number is LLNL-CONF-413264. This work has been supported by the National Science Foundation Science and Technology Center for Adaptive Optics, managed by the University of California at Santa Cruz under cooperative agreement No. AST - 9876783.

References

1. L. A. Poyneer and J.-P. Véran, "Optimal modal Fourier transform wave-front control," *J. Opt. Soc. Am. A* **22**, 1515–1526 (2005).
2. L. A. Poyneer and D. Dillon, "MEMS Adaptive Optics for the Gemini Planet Imager: control methods and validation," (2008), *Proc. SPIE* **6888**, p. 68880H.
3. J. W. Evans, K. Morzinski, S. Severson, L. Poyneer, B. Macintosh, D. Dillon, L. Reza, D. Gavel, D. Palmer, S. Olivier, and P. Bierden, "Extreme adaptive optics testbed: performance and characterization of a 1024-MEMS deformable mirror," (2006), *Proc. SPIE* **6113**, p. 61130I.
4. C. R. Vogel and Q. Yang, "Modeling, simulation, and open-loop control of a continuous facesheet MEMS deformable mirror," *J. Opt. Soc. Am. A* **23**, 1074–1081 (2006).